Tyr is Responsible for the *Cctq1a* QTL and Links Developmental Environment to Central Corneal Thickness Determination

Kacie J. Meyer[1§], Demelza R. Larson[1§], S. Scott Whitmore[2], Carly J. van der Heide[1,2], Adam Hedberg-Buenz[1,3], Laura M. Dutca[3], Swanand Koli[4], Nicholas Pomernackas[1], Hannah E. Mercer[1], Maurisa N. Mansaray[1], William J. Paradee[5], Kai Wang[6], K. Saidas Nair[4,7], Todd E. Scheetz[2], and Michael G. Anderson[1,2,3*]

[1]Department of Molecular Physiology and Biophysics, University of Iowa, Iowa City, Iowa; [2]Department of Ophthalmology and Visual Sciences, University of Iowa, Iowa City, Iowa; [3]Center for the Prevention and Treatment of Visual Loss, Iowa City VA Health Care System, Iowa City, Iowa; [4]Department of Ophthalmology, University of California, San Francisco, California; [5]Genome Editing Core Facility, University of Iowa, Iowa City, Iowa; [6]Department of Biostatistics, University of Iowa, Iowa City, Iowa; [7]Department of Anatomy, University of California, San Francisco, California

[§]Equal contribution

*Corresponding author: Dr. Michael G. Anderson, Department of Molecular Physiology and Biophysics, 3111 Medical Education and Research Facility, 375 Newton Road, Iowa City, IA 52242, (319) 335-7839 (telephone), (319) 335-7330 (FAX), michael-g-anderson@uiowa.edu

Abstract

Central corneal thickness is a quantitative trait with important associations to human health. In a phenotype-driven approach studying corneal thickness of congenic derivatives of C57BLKS/J and SJL/J mice, the critical region for a quantitative trait locus influencing corneal thickness, *Cctq1a*, was delimited to a 10-gene interval. Exome sequencing, RNAseq, and studying independent mutations eliminated multiple candidate genes and confirmed one. Though the causative gene, *Tyr*, has no obvious direct function in the transparent cornea, studies with multiple alleles on matched genetic backgrounds, both in isolation and genetic complementation crosses, confirmed allelism of *Tyr-Cctq1a*; albino mice lacking *Tyr* function had thin corneas. Albino mice also had increased axial length. Because albinism exposes eyes to increased light, the effect of dark-rearing was tested and found to rescue central corneal thickness. In sum, the results point to an epiphenomenon; developmental light exposure interacts with genotype as an important determinate of adult corneal thickness.

39 **Introduction**

40

41 Central corneal thickness has important associations with ocular disease, but its natural
42 determining factors remain predominately elusive. The cornea consists of three cellular layers
43 (an outermost epithelium, middle stroma, and innermost endothelium) separated by two thinner
44 basement membranes. The combined central thickness of these layers (central corneal
45 thickness, CCT) increases rapidly through infancy and early childhood, reaches adult values in
46 pre-teen ages, and remains relatively stable thereafter, with eventual modest age-related
47 thinning[1-3, 4]. For largely unknown reasons, average CCT can vary by dozens of microns
48 between ethnicities[4,5]. Thin CCT is associated with several corneal diseases, such as corneal
49 dystrophy, brittle cornea syndrome, keratoconus, and cornea plana; diseases of connective
50 tissue, such as Marfan syndrome, Ehlers-Danlos syndrome, Loeys-Dietz syndrome, and
51 osteogenesis imperfecta; and at least two diseases in which the nature of, and/or reason for, the
52 association is unclear, including myopia and primary open angle glaucoma[6].

53

54 CCT is a highly heritable trait[7,8], leading to many genetic studies. Variants influencing CCT have
55 been identified from familial studies of Mendelian syndromes and GWAS of various large
56 populations[9-12]. From these studies, some themes have begun to emerge. For example, some
57 of the same CCT loci are identified in both multigenic and Mendelian disease studies[10,13,14]. It
58 has also been common to identify variants related to collagen matrix integrity[10,12,14,15]. However,
59 it is also clear that much remains unknown. Among the known associations, most known SNPs
60 occur in non-coding regions, and the nearest genes typically have no obvious link to known
61 structural components of the cornea[15]. It is also clear that many important genes remain to be
62 discovered. Known SNPs give rise to a SNP-based heritability estimate of 42.5% and account
63 for only 14.2% of the CCT variance[9].

64

65 Here, an unique approach complementary to others is undertaken using inbred mouse strains to
66 identify quantitative trait loci (QTL) that influence CCT[16,17]. Similar to humans, there is natural
67 variation of CCT among inbred mouse strains[18]. Previous work using a quantitative approach
68 with intercrosses between two such strains (C57BLKS/J [KS] mice with thin corneas and SJL/J
69 [SJL] mice with thick corneas) identified the first CCT QTL, *Central corneal thickness QTL 1*
70 (*Cctq1*) on mouse chromosome 7[16]. Here, *Cctq1* was resolved into two closely linked regions,
71 *Cctq1a* and *Cctq1b*, which each influence CCT. Through multiple genetic approaches, a
72 mutation in the tyrosinase gene (*Tyr*) is identified as causative of the *Cctq1a* phenotype, which
73 appears to influence CCT via an epiphenomenon dependent on developmental light exposure.
74

75 **Results**

76

77 ***Cctq1* contains two adjacent interacting QTL**

78 The original 95% Bayesian credible interval of *Cctq1* spanned a 38.3 cM region on chromosome
79 7 (34.1 cM – 72.4 cM)[16]. To reduce this interval, recombination mapping was used with 92
80 recombinant N4 intercross mice. However, the interval was originally recalcitrant to division—
81 more than one interval conferred the increased CCT phenotype. This suggested that there was
82 too much genetic heterogeneity for this trait at the N4 generation, potentially including the
83 presence of more than one CCT-regulating gene within or near *Cctq1*. To address these
84 possibilities, the original F2 dataset was subjected to additional evaluations while backcrossing
85 of the congenic mice to the N10 generation was continued.

86

87 The original analysis of (KS X SJL) F2 mice was based upon a significance threshold
88 determined empirically by stratified permutation testing with 1000 permutations[16,19], and did not
89 identify any loci that significantly interacted with *Cctq1*. Prompted by the recombination

90 mapping, the dataset was re-examined by performing a pairwise scan of the markers on
91 chromosome 7 using scantwo analysis with R/qtl[19,20]. Of the possible interactions, the markers
92 that produced the highest LOD scores were *D7Mit31* and *rs13479535* (Figure 1A; full LOD
93 score = 10.33, interactive LOD score = 5.05). *D7Mit31* lies within the 95% Bayes credible
94 interval of *Cctq1*; *rs13479535* is 2 cM distal to the end of the interval at 74.3 cM. The putative
95 linked loci were subsequently subjected to multiple regression analysis in which each locus and
96 the interaction component were sequentially dropped from the 2-QTL model. This analysis
97 indicated that both loci and their interaction had significant contributions to the model
98 (Supplementary Data 1). The QTL at *D7Mit31* was responsible for 31% of the phenotypic
99 variability while the QTL at *rs13479535* accounted for another 24% of the variability. These data
100 indicate that both loci are true QTL. *Cctq1* was thus resolved into two QTL, *Cctq1a* (95% Bayes
101 credible interval: *D7Mit318–D7Mit220*, spanning 49.0 cM, peak at *D7Mit31*), and *Cctq1b* (95%
102 Bayes credible interval: *D7Mit105–rs13479545*, spanning 74.3 cM, peak at *rs13479535*; Figure
103 1B).
104
105 To reduce genetic heterogeneity, N4 mice were further backcrossed onto the KS background to
106 the N10 generation. Because the congenic interval was relatively large, a panel of six markers
107 was used at each generation of backcrossing to keep the interval intact. At generation N10,
108 congenic mice were intercrossed, recombination within the interval was allowed, and mice with
109 all nine genetic combinations of *Cctq1a* and *Cctq1b* were phenotyped for CCT (Table 1).
110 Congenic control mice (KS.SJL-$Cctq1a^{KS}$,$Cctq1b^{KS}$) had a CCT indistinguishable from inbred
111 KS mice (94.8± 2.4 μm vs. 94.5 ± 3.2 μm, respectively; one-way ANOVA with Tukey post-test;
112 Table 1). Congenic mice with SJL genotypes at *Cctq1a* (*i.e.*, KS.SJL-$Cctq1a^{SJL}$) had significantly
113 thinner corneas than inbred KS mice (87.9 ± 3.8 μm; n = 39; p < 0.001; Student's two-tailed *t*-
114 test) independent of the genotype at *Cctq1b* (n = 13 and p < 0.05 for each of three genotypes at
115 *Cctq1b*; one-way ANOVA with Tukey post-test; Table 1; Supplementary Data 2). The difference

116 in thickness mediated by *Cctq1a* is predominantly due to the thickness of the stroma (Δ 9.6 μm,
117 $p < 0.001$; Student's two-tailed *t*-test), though there is a small (Δ 1.2 μm) and marginally
118 significant ($p = 0.022$ Student's two-tailed *t*-test) decrease in thickness of the epithelium as well.
119 Congenic mice with KS genotypes at *Cctq1a* and SJL genotypes at *Cctq1b* (i.e., KS.SJL-
120 $Cctq1a^{KS}$,$Cctq1b^{SJL}$) also had significantly thinner corneas (90.8 ± 2.6 μm; $n = 13$ mice; $p < 0.05$;
121 one way ANOVA with Tukey post-test) than inbred KS mice (Table 1, Supplementary Data 2).
122 No other genetic combinations caused significant changes in CCT compared to inbred KS
123 controls. As predicted from the analysis of the original F2 Dataset with R/qtl, these data with
124 congenic mice independently support that both *Cctq1a* and *Cctq1b* are true QTL capable of
125 altering the phenotypic variability of CCT on a uniform genetic background.
126

127 **Mapping of *Cctq1a* using recombination mapping and sub-congenics**

128 Because of its larger effect, initial efforts were focused on fine-scale mapping for *Cctq1a*. To
129 identify the gene underlying *Cctq1a*, *Cctq1a*-recombinant N10F2 mice, with KS genotypes at
130 *Cctq1b*, were used to narrow the critical region. From this recombination analysis, the gene
131 underlying *Cctq1a* was deduced to be between SNP markers *rs108403472* at 48.51 cM and
132 *rs6247100* at 50.26 cM. Simultaneously, sub-congenic mice were created by continued
133 backcrossing of the KS.SJL-$Cctq1a^{HET}$;$Cctq1b^{KS}$ N10 mice. Eyes of N10 congenic mice were
134 overtly healthy, differing only in pigmentation between genotypes (Supplementary Data 2). At
135 N12, *Cctq1a* was physically reduced to a 15.9 cM region (KS.SJL-*Cctq1a(15.9cM)*) flanked by
136 *D7mit347* and *D7mit321* and characterized by an association of SJL homozygosity with
137 decreased CCT (87.6 ± 2.3 μm vs. 76.8 ± 2.4 μm, $n = 15$ mice per genotype, $p < 0.001$,
138 Student's two-tailed *t*-test). At N15, *Cctq1a* was physically reduced to a 9.9 cM region (KS.SJL-
139 *Cctq1a(9.9cM)*) flanked by *rs3672782* and *D7mit321*; again characterized by an association of
140 SJL homozygosity with decreased CCT (91.6 ± 2.2 μm vs. 80.7 ± 2.9 μm, $n = 7$ mice per
141 genotype, $p < 0.001$, Student's two-tailed *t*-test). One N15F2 mouse harbored a recombination

142 event within the minimal sub-congenic interval. The phenotype of this mouse indicated the gene
143 underlying *Cctq1a* lies proximal to marker *rs13479393* (Figure 2). Using this recombinant
144 mouse in a progeny test, additional intercrossing to generation N15F7 confirmed the distal
145 breakpoint proximal to marker *rs13479393* at 49.65 cM, again characterized by an association
146 of SJL homozygosity with decreased CCT (85.7 ± 1.6 μm vs. 94.4 ± 3.3 μm, n = 8–10 mice per
147 genotype; $p < 0.001$, Student's two-tailed t-test; Figure 3A; Supplementary Data 3–5).
148
149 In sum, physical recombination mapping utilizing multiple generations of congenic and sub-
150 congenic mice conclusively indicated that the gene underlying *Cctq1a* lies on chromosome 7
151 between markers *rs108403472* at 48.51 cM and *rs13479393* at 49.32 cM, a 0.81 cM region
152 containing the entirety of eight RefSeq genes (*Vmn2r78*, *Vmn2r79*, *Nox4*, *Tyr*, *Grm5*, *Ctsc*,
153 *Rab38*, and *Tmem135*), the 3' portion of one gene (*Vmn2r77*), and the 5' portion of one gene
154 (*Fzd4*) (Figure 2).
155
156 **Candidate identification and prioritization**
157 To identify all the possible exonic variants within the *Cctq1a* critical region, whole exome
158 sequencing was conducted on KS and SJL inbred mice. In the entire exome, 15,261 missense,
159 frameshift, and splice-site mutations were found between KS and SJL (Supplementary Data 6).
160 There were six amino acid altering variants within the *Cctq1a* critical region, located within
161 *Vmn2r79* (A223T, L243M, T257I, I265V), *Tyr* (C103S), and *Fzd4* (F27L). Vomeronasal receptor
162 genes, such as *Vmn2r79*, have an increased rate of coding sequence variants [21] and the four
163 altered residues between KS and SJL in *Vmn2r79* are poorly conserved. The amino acid
164 change in *Tyr* from cysteine to serine is the albinism-causing Tyr^c allele conferred by the albino
165 SJL strain. The *Fzd4* amino acid variant is within the signal sequence of the protein; KS mice
166 conferred the phenylalanine amino acid residue (the same residue as C57BL/6J mice) while
167 SJL mice conferred the mammalian-conserved leucine residue.

168

169 Transcriptional profiling was additionally used to prioritize candidates. Using previously
170 published microarray data comparing adult corneal RNA expression profiles in KS and SJL
171 mice[18], *Nox4*, *Ctsc*, *Rab38*, *Tmem135*, and *Fzd4* were all present in the adult cornea; there was
172 no evidence for adult corneal expression of *Vmn2r77*, *Vmn2r78*, *Vmn2r79*, *Tyr*, or *Grm5*. Of
173 those expressed, *Nox4, Ctsc, and Fzd4* showed differential expression between the two strains.
174 *Nox4* and *Ctsc* were both down-regulated 2.5-fold in SJL, while *Fzd4* was up-regulated 1.6-fold
175 in SJL.

176

177 Additionally, RNAseq was performed on corneas of 3-week-old KS.SJL-*Cctq1a(15.9cM)*^{SJL}
178 N12F3 mice. Analysis was focused on three comparisons: 1) KS.SJL-*Cctq1a(15.9cM)*^{SJL} vs. KS
179 (experimental, identifying genes with altered corneal expression in the congenic interval), 2)
180 KS.SJL-*Cctq1a(15.9cM)*^{SJL} vs. KS.SJL-*Cctq1a(15.9cM)*^{KS} (experimental, also identifying genes
181 with altered corneal expression in the congenic interval), and 3) KS.SJL-*Cctq1a(15.9cM)*^{KS} vs.
182 KS (control, identifying genes in the background of the congenic strain with altered corneal
183 expression not associated with the congenic interval) (Supplementary Data 7). In each
184 comparison, genes were first filtered for those with a Q-value ≤ 0.001 and a FPKM ≥ 1 in at
185 least one of the strains. Gene lists were subsequently compared to one another, identifying 87
186 genes consistently altered in both experimental comparisons but not in the control comparison
187 (Supplementary Data 7). Among these 87, only one was localized to the *Cctq1a* critical region,
188 *Ctsc*, which was modestly (-0.8 $\log_2$ fold) but consistently and significantly ($p = 5 \times 10^{-5}$; $Q =$
189 0.0009) down regulated in comparing the SJL allele to the KS allele. Web Gestalt[22] was used for
190 over-representation analysis comparing the list of 87 differentially expressed genes to a
191 background list of all genes expressed in the cornea with a FPKM ≥ 1 in any strain. Results of
192 the analysis indicate a strong signal for several collagen-related categories (fibrillar collagen
193 trimer, abnormal cutaneous collagen fibril morphology, collagen biosynthesis and modifying

194 enzymes, collagen degradation, etc.), extracellular-matrix-related categories (extracellular
195 matrix component, ECM proteoglycans, degradation of the extracellular matrix, etc.) and ocular-
196 related categories (decreased corneal stroma thickness, abnormal corneal epithelium
197 morphology, abnormal cornea morphology, and abnormal eye morphology) (Supplementary
198 Data 8).
199
200 **Functional tests of lead candidates**
201 Based on candidate prioritization criteria, *Fzd4* and *Ctsc* were initially considered the top
202 candidates. To test the influence of *Fzd4* on CCT, we tested a strain with a targeted mutation of
203 *Fzd4* (B6;129-$Fzd4^{tm1Nat}$/J) on a segregating B6 and 129 background[23]. $Fzd4^{tm1Nat}$ homozygotes
204 had a chocolate coat color not expected from either background. This observation is meaningful
205 as the gene responsible for this phenotype, *Rab38*, is physically near *Fzd4* and within the *Cctq1*
206 critical region, i.e., the strain is likely a double mutant for *Fzd4* (genotype verified) and *Rab38*
207 (mutation unknown). However, there was no correlation between $Fzd4^{tm1Nat}$ genotype and CCT
208 (p = 0.819; one-way ANOVA comparing all three genotypes among littermates; Figure 3B;
209 Supplementary Data 3–5). In genetic complementation crosses, $Fzd4^{tm1Nat}$ mutation
210 complemented the congenic interval ([$Fzd4^{WT}$/$Cctq1a^{SJL}$ F1] vs. [$Fzd4^{HET}$/$Cctq1a^{SJL}$ F1]; p =
211 0.528; Student's two-tailed t-test; n = 4-6 per genotype; Figure 3C; Supplementary Data 3–5).
212 The complementation cross also highlighted the coat color phenotype associated with the
213 $Fzd4^{tm1Nat}$ mutation, with $Fzd4^{WT}$/$Cctq1a^{SJL}$ F1 mice (Tyr^{HET}) having a black coat color with
214 normally pigmented eyes and $Fzd4^{HET}$/$Cctq1a^{SJL}$ F1 mice (Tyr^{HET}) having an unmistakable
215 lightened ("light chocolate") coat color and light brown irides instead of brown (Supplementary
216 Data 9). Therefore, *Fzd4* was ruled out as causative of the *Cctq1a* phenotype, and *Rab38*
217 further deprioritized as a candidate.
218

219 To test the influence of *Ctsc* on CCT, we imported a strain with a targeted mutation of *Ctsc*
220 (B6.Cg-*Ctsc*^{tm1Ley}) on an N10 congenic B6 background[24]. Because the targeted mutation was
221 generated on an albino 129 background, and *Ctsc* is physically linked to *Tyr*, *Ctsc*^{tm1Ley}
222 homozygotes are albino, i.e., the strain is a double mutant for *Ctsc* and *Tyr*. This is meaningful
223 because the SJL/J strain is albino and the *Tyr*^{c} mutation is within the KS.SJL-*Cctq1a* congenic
224 interval. Homozygotes had a statistically significant decrease in CCT compared to littermate
225 controls ($p < 0.002$ for albino *Ctsc*^{tm1Ley} vs. pigmented *Ctsc*^{HET}; $p < 0.002$ for albino *Ctsc*^{tm1Ley} vs.
226 pigmented *Ctsc*^{WT}; one-way ANOVA with Tukey post-test comparing all three genotypes among
227 littermates; n=10–12 mice per genotype; Figure 3D; Supplementary Data 3–5). In genetic
228 complementation crosses, *Ctsc*^{tm1Ley} failed to complement *Cctq1a*^{SJL} ($p < 0.001$ for pigmented
229 [*Ctsc*^{tm1Ley}/*Cctq1a*^{KS} F1] vs. albino [*Ctsc*^{tm1Ley}/*Cctq1a*^{SJL} F1]; Student's two-tailed *t*-test; n = 10–
230 11 mice per genotype; Figure 3E; Supplementary Data 3–5). Therefore, *Ctsc or Tyr* were
231 determined to be causative of the *Cctq1a* phenotype.
232
233 To differentiate *Ctsc* and *Tyr* as the causative mutation, independent alleles on a pure B6
234 background were assessed. To test *Ctsc*, four new mutations predicted to result in null protein
235 were generated in B6 mice with CRISPR-Cas9 technology (Supplementary Data 10). To test
236 *Tyr*, a well-known spontaneous mutation that was commercially available, *Tyr*$^{c-2J}$, was
237 analyzed[25,26]. There was no association between *Ctsc*^{KO} genotype and CCT (p = 0.237; one-
238 way ANOVA comparing all three genotypes among littermates; n = 9–17 mice per group; Figure
239 3F; Supplementary Data 3-5). In genetic complementation crosses with the congenic strain, the
240 *Ctsc*^{tm1Mga} mutation (46bp-deletion in the coding sequence of exon 1 leading to no detectable
241 CTSC protein; Supplementary Data 10) complemented the congenic phenotype (p = 0.696;
242 Student's two-tailed *t*-test; n = 8–12 mice per group; Figure 3G; Supplementary Data 3–5). In
243 contrast, albino *Tyr*$^{c-2J}$ mice had decreased CCT relative to pigmented B6 ($p < 0.001$; Student's
244 two-tailed *t*-test; n = 9–10 mice per group; Figure 3H; Supplementary Data 3–5). In genetic

245 complementation crosses with the congenic strain, the *Tyr*$^{c\text{-}2J}$ mutation failed to complement the
246 congenic phenotype ($p < 0.001$ for pigmented [*Cctq1a*^{KS}/*Tyr*$^{c\text{-}2J}$ F1] vs. albino [*Cctq1a*^{SJL}/*Tyr*$^{c\text{-}2J}$
247 F1]; Student's two-tailed *t*-test; $n = 8$ mice per genotype; Figure 3I; Supplementary Data 3–5).
248 Thus, only *Tyr* mutation was left as a feasible candidate for *Cctq1a*.
249
250 CRISPR-Cas9 technology was also used to generate new *Tyr* mutations on a C57BL/6J
251 background (Supplementary Data 11). One allele was selected for propagation, *Tyr*^{tm4Mga}, an
252 albinism-causing 4bp-deletion in the coding sequence of exon 1 that is predicted to cause a
253 frameshift leading to a premature stop codon and RNA-mediated decay; i.e., a presumed null
254 mutation. *Tyr*^{tm4Mga} mice had a significantly thinner cornea than littermate controls ($p < 0.002$ for
255 *Tyr*^{WT} vs. *Tyr*^{tm4Mga}; $p < 0.002$ for *Tyr*^{HET} vs. *Tyr*^{tm4Mga}; one-way ANOVA with Tukey post-test
256 comparing all three genotypes among littermates; $n = 6$–10 mice per genotype; Figure 4;
257 Supplementary Data 5 and 12). Thus, a presumed null allele of *Tyr* caused the same albinism
258 and thinning of CCT as found for the *c* and *c-2J* alleles.
259
260 **Mechanism of *Tyr* function on CCT**
261 In considering the possible mechanism through which *Tyr* might influence CCT, three
262 hypotheses were tested:
263
264 The first candidate mechanism centered on the role of DOPA, which is a cofactor in the
265 oxidation of tyrosine by TYR, leading to melanin production[27], and a substrate for tyrosine
266 hydroxylase (TH), leading to dopamine synthesis. Dopamine is considered a key molecule in
267 ocular growth[28,29], and mice with a conditional knock-out of *Th* in the retina have previously
268 been shown to have decreased CCT[30]. Rationalizing that some DOPA may normally escape
269 from pigment producing cells to influence CCT via a TH-dependent mechanism, we tested
270 whether providing supplemental DOPA in the drinking water of albino mice would rescue the

271 decreased CCT associated with albinism. No statistically significant effect was observed (Figure
272 5; Supplementary Data 5), discounting the hypothesis that a DOPA deficit was rate-limiting for
273 CCT determination in *Tyr* mutant mice.
274
275 The second candidate mechanism revolves around the possibility of a gene-environment
276 interaction involving temperature and light. In this series of experiments, mice were reared in
277 environmental control chambers in combinations of different temperatures and light cycles.
278 Cohorts included pigmented B6, albino $Tyr^{c\text{-}2J}$, and the temperature sensitive himalayan
279 mutation (B6.Cg-$Tyr^{c\text{-}h}$/J)[31,32]. At ambient temperatures, $Tyr^{c\text{-}h}$ homozygotes are only partially
280 pigmented on the coolest parts of the body (such as the ears, nose, tail, and eyes) and CCT is
281 intermediate between B6 and $Tyr^{c\text{-}2J}$ mice (Supplementary Data 5, 13, and 14). For CCT of mice
282 raised at ambient temperature, genetic complementation tests again confirmed the influence of
283 *Tyr*-mediated albinism on CCT (p = 0.337 for [pigmented B6 x $Tyr^{c\text{-}h}$ F1] vs. [pigmented B6 x
284 $Tyr^{c\text{-}2J}$ F1]; $p < 0.002$ for [pigmented B6 x $Tyr^{c\text{-}h}$ F1] vs. [albino $Tyr^{c\text{-}h}$ x $Tyr^{c\text{-}2J}$ F1]; and $p < 0.002$
285 for [pigmented B6 x $Tyr^{c\text{-}2J}$ F1] vs. [albino $Tyr^{c\text{-}h}$ x $Tyr^{c\text{-}2J}$ F1]; one-way ANOVA with Tukey post-
286 test; n = 4–14 mice per group, Supplementary Data 5). At decreased temperatures $Tyr^{c\text{-}h}$
287 homozygotes can generate pigment more broadly, and at increased temperatures the albinism
288 is accentuated (Supplementary Data 13 and 14).
289
290 Regarding temperature, comparison of B6.$Tyr^{c\text{-}h}$ mice, as well as B6 and B6.$Tyr^{c\text{-}2J}$ controls,
291 raised at 10°C vs. 32°C in environmental control chambers with a standard light cycle, showed
292 that CCT followed pigment status; the thin CCT of hypopigmented $Tyr^{c\text{-}h}$ mice reared at
293 increased temperature (i.e., lower TYR activity) was rescued by rearing the $Tyr^{c\text{-}h}$ mice at
294 decreased temperature (i.e., higher TYR activity; $Tyr^{c\text{-}h}$ at 32°C vs. $Tyr^{c\text{-}h}$ at 10°C; Δ 10.9 μm; p
295 < 0.001; n = 13–15 mice per condition; one-way ANOVA with Sidak test; Figure 6;
296 Supplementary Data 5). In testing the effect of temperature on corneal thickness in controls,

297 there was a small (Δ 2.8 μm) and nominally significant (p = 0.03) decreased CCT in mice raised
298 at 10ºC compared to mice raised at 32ºC when considering all C57BL/6J and *Tyr*$^{c\text{-}2J}$ mice
299 across the experiment (n = 16 mice vs. n = 19 mice, Type II ANOVA) and there was no
300 interaction between genotype and temperature. In sum, changing environmental temperature
301 changed CCT of the *Tyr*$^{c\text{-}h}$ mice as predicted.
302
303 Regarding light, comparison of B6.*Tyr*$^{c\text{-}h}$ mice, as well as B6 and B6.*Tyr*$^{c\text{-}2J}$ controls, raised at
304 10°C vs. 32°C in environmental control chambers with dark-rearing of mice from conception to
305 10–15 weeks of age rescued the thin CCT phenotype associated with albinism (p < 0.001 for
306 [*Tyr*$^{c\text{-}h}$ at 32°C standard light] vs. [*Tyr*$^{c\text{-}h}$ at 32°C dark rear]; p < 0.03 for [*Tyr*$^{c\text{-}2J}$ at 10°C standard
307 light vs. *Tyr*$^{c\text{-}2J}$ at 10°C dark rear]; p < 0.001 for [*Tyr*$^{c\text{-}2J}$ at 32°C standard light vs. *Tyr*$^{c\text{-}2J}$ at 32°C
308 dark rear]; n = 5–16 per condition; one-way ANOVA with Sidak test; Figure 6; Supplementary
309 Data 5). Rearing pigmented B6 mice in constant light is known to lead to an increase in axial
310 length[33]. OCT examinations of independent cohorts of C57BL/6J and *Tyr*$^{c\text{-}2J}$ mice for the
311 purpose of measuring axial length show that *Tyr*$^{c\text{-}2J}$ mice have a 65.6 μm greater axial length on
312 average compared to C57BL/6J mice (3.453 mm vs. 3.388 mm, respectively; p < 0.001,
313 Student's two-tailed t-test; n = 10 male and 10 female mice per strain; Figure 7).
314
315 **Discussion**
316 Using a phenotype-driven quantitative genetic analysis of CCT, physical mapping led to
317 identification of a small critical region containing 10 genes, of which we ruled out three (*Fzd4*,
318 *Rab38*, *Ctsc*) and found via an analysis of a *Tyr* allelic series (*c*, *c-2J*, *c-h*) that *Tyr* is the
319 causative gene underlying the *Cctq1a* QTL. *Tyr* is by no means an unknown gene—it was in
320 fact one of the first known mammalian genes whose initial discovery predates the word
321 "gene"[27,34,35]. However, *Tyr* was a surprising gene to find linked to CCT. TYR is an oxidase
322 whose only known biological role relates to melanin synthesis[27,36]. Although there are small

323 numbers of pigmented cells in the corneal limbus, the cornea is by and large not only non-
324 pigmented, but transparent. Furthermore, previously published data indicate that *Tyr* is not even
325 expressed in the adult cornea[18], which is consistent with the current study which also found
326 near-zero expression in the cornea at 3 weeks of age (RNA-Seq max expression ~1.3 FPKM;
327 Supplementary Data 7). Thus, there is no molecular rationale for proposing that TYR has a
328 direct function in corneal cells. If not for the current experiments, there would also be sparse
329 biological rationales for proposing that TYR might influence corneal anatomy through any
330 mechanism. Regardless, the current agnostic QTL study led to the conclusion that *Tyr*
331 contributes to the primary genetic influence on CCT, at least in the context of KS x SJL hybrids.
332 Experiments using multiple alleles on matched genetic backgrounds, in isolation and genetic
333 complementation crosses, conclusively confirmed allelism of *Tyr-Cctq1a*; albino mice lacking
334 TYR function have thin corneas. Rationalizing that albinism would expose the developing eye to
335 increased light, one of the mechanistic experiments performed here compared the effect of
336 dark-rearing on the CCT of albino vs. pigmented C57BL/6J mice. The results showed that the
337 thin CCT phenotype of albino B6.$Tyr^{c\text{-}h}$ mice raised at 32°C and B6.$Tyr^{c\text{-}2J}$ mice was rescued by
338 dark-rearing. Thus, we are led to propose an epiphenomenon, whereby developmental light
339 exposure interacts with genotype as an important determinate of corneal thickness.
340
341 All current CCT measurements were done with mice 10–15 weeks of age, which is slightly past
342 the age at which the cornea of B6 mice reaches its final adult thickness (~P55)[37]. Transcriptomic
343 changes in the cornea related to *Tyr* genotype were detectable at 3 weeks of age. Thus, the
344 timeframe for when *Tyr* can impact the cornea is presumably during anterior chamber
345 development at some point preceding 3 weeks of age. Two mechanisms, which are both
346 conjectural, might feasibly contribute to this early acting phenomenon. 1) Corneal development
347 might be a component of refractive development. Emmetropization typically occurs in the first
348 months following eyelid opening, with impacts from both the amount of light and its focus on the

349 retina[33,38]. Thus, it is feasible that albinism could in effect cause blur (from light not being
350 absorbed by melanin and reflecting within the eye), which induces relative myopia and CCT
351 thinning with rearing in normal lights, but not in dark-rearing. 2) Corneal development might be
352 influenced by central or corneal circadian outputs. Circadian outputs arise from both central and
353 peripheral clocks, with the suprachiasmatic nucleus (SCN) being a central master pacemaker
354 that receives light signals from retinal ganglion cells and subsequently coordinates phasing to
355 peripheral tissues[39,40]. Notably, the SCN receives retinal input from the retinohypothalamic tract,
356 which is known to be expanded in albinos[41-43]. Thus, one possibility is that factors increasing
357 SCN output (such as albinism or cycling light conditions) might lead to decreased CCT and
358 those decreasing the signaling (such as dark rearing) might lead to increased CCT. Refractive
359 and circadian mechanisms could also be acting in an intertwined way[44]. Additional experiments
360 are needed to distinguish these, and possibly other, mechanisms relevant to our current
361 findings.
362
363 A leading candidate for contributing to the molecular mechanism causing thin CCT in albino
364 mice was DOPA, which is a cofactor for TYR[27,36], a substrate for TH leading to dopamine
365 (reviewed in [28]), and an endogenous ligand for the G-protein-coupled receptor GPR143[45] .
366 DOPA can modulate refractive development[27, 29, 40] and the circadian system[46], as well
367 development of multiple ocular tissues[47,48]. Notably, mice with a conditional knock-out of *Th* in
368 the retina have decreased CCT[30]. The current experiments with *Tyr* mutant mice were not able
369 to detect a role for DOPA in influencing CCT of these albino strains, though an important caveat
370 to point out is that only a single dosing schedule for DOPA supplementation was currently
371 tested.
372
373 It is unclear whether albinism or pigmentation influences CCT in humans, though our current
374 experiments suggest this is likely. In humans, loss of function mutations in *TYR* cause

375 oculocutaneous albinism type 1 (OCA 1)[36,49]. It's unclear from the literature if humans with OCA
376 1 have decreased CCT; it may be difficult to ascertain because of relatively small patient
377 populations and confounding variables such as eye rubbing[50].
378
379 The current study has several implications with respect to mouse genetics and mouse models of
380 disease: 1) The results highlight the potential for environmental influences on ocular
381 development, which have been quantitated here for CCT, but may extend to other tissues as
382 well. 2) The results indicate that albino mice should be tested for potentially being a naturally
383 occurring model of myopia. 3) Because CCT is a complex trait, there is little reason to suspect
384 that different inbred albino mouse strains would necessarily have the thinnest CCT in
385 comparison to other inbred strains that are pigmented[51], only that they would have thinner CCT
386 as albino mice compared to pigmented mice *within* an inbred strain. However, for any
387 experiment using such an albino strain, or cohorts in which an allele such as the common Tyr^{c}
388 allele is segregating, attention to the possibility of environmental influences is warranted. 4) *Tyr*
389 has been linked with many ophthalmic traits in mice[41-43,47,52-57]; in some instances, a
390 consideration of gene-environment interactions in the mechanism of these various models may
391 be warranted. And finally, 5) our study uncovers a genetic peculiarity. *Cctq1* was originally
392 reported as a single QTL on chromosome 7, detected in an F2 intercross of KS and SJL inbred
393 mice[16]. In studies of successive generations of congenic mice, N4F2 mice heterozygous for the
394 *Cctq1* alleles showed the original differential phenotype (over-dominant, *increased* CCT
395 compared to littermate controls)[16], whereas in N10–N15 intercrosses, mice homozygous for the
396 SJL allele showed the differential phenotype (recessive, *decreased* CCT compared to littermate
397 controls). As the sub-congenics were intercrossed and analyzed for CCT, KS.SJL-
398 $Cctq1a^{SJL};Cctq1b^{KS}$ mice consistently had thinner corneas than KS.SJL-$Cctq1a^{KS};Cctq1b^{KS}$
399 mice of the same generation, but there were also fluctuations in absolute value related to
400 generation and interval size. The likely explanation for these observations is that there was

401 more than one CCT-modifying gene in the original *Cctq1* interval, which was in fact found to be
402 the case by the resolution of *Cctq1* into *Cctq1a* and *Cctq1b*. This is consistent with the findings
403 of human GWAS, indicating that there are likely hundreds of CCT-influencing genes dispersed
404 throughout the genome, many of which will be physically close to one another. In mice, it is
405 known that as a locus is narrowed using congenics, genes can be segregated away from
406 nearby modifiers and the overall phenotype of the original QTL can be reduced, disappear, or
407 reverse its apparent effect[58-60]. The current data seem to exemplify this phenomenon.
408
409 In summary, our phenotype-driven genetic study of CCT identified *Tyr* as a significant regulator
410 of CCT in mice. The molecular findings of this study were unexpected. We propose that the
411 results can be explained by an epiphenomenon whereby a gene:environment interaction; i.e.,
412 *Tyr*-mediated albinism allowing increased exposure of the eye to light has an important
413 influence on corneal development.
414
415 **Materials and Methods**
416
417 **Experimental animals**
418 All animals were treated in accordance with the ARVO Statement for the Use of Animals in
419 Ophthalmic and Vision Research. The majority of mice were housed and bred at the University
420 of Iowa Research Animal Facility with approval for experimental protocols conferred by the
421 Institutional Animal Care and Use Committee of the University of Iowa. Two cohorts of mice, the
422 C57BL/6J (JAX Stock No. 000664) and B6.Cg-Tyr^{c-2J}/J (JAX Stock No. 000058) used for in vivo
423 axial length measurements (Figure 7) were purchased from The Jackson Laboratory at 10-
424 weeks-old and subsequently housed at the University of California San Francisco until 12-
425 weeks-old with approval for experimental protocols conferred by the Institutional Animal Care
426 and use Committee at the University of California San Francisco. Mouse strains used in this

427 study include: SJL/J (Stock No. 000686), C57BLKS/J (JAX Stock No. 000662), C57BL/6J (JAX
428 Stock No. 000664), B6.Cg-*Tyr*$^{c\text{-}2J}$/J (JAX Stock No. 000058), B6;129-*Fzd4*^{tm1Nat}/J (JAX Stock
429 No. 012823), B6.Cg-*Tyr*$^{c\text{-}h}$/J (JAX Stock No. 000104; Imported from Dr. Brian Brooks at the
430 NIH), B6.Cg-*Ctsc*^{tm1Ley} (Imported from Dr. Christine Pham at Washington University), KS.Cg-
431 SJL^{Cctq1}, B6-*Ctsc*^{tm1Mga}, and B6-*Tyr*^{tm4Mga}. All experiments included male and female mice.
432

433 **Chromosome 7 QTL analysis**

434 The chromosome 7 quantitative trait locus analysis was performed with R/qtl, using the two-
435 dimensional genome-wide scan (scantwo). Significance thresholds were determined empirically
436 by permutation testing, using 1000 permutations. The validity of a multiple QTL model was
437 tested by performing a multiple regression analysis. Phenotypic variance was estimated and the
438 full model was statistically compared to reduced models in which one QTL was dropped.
439

440 **Constructing congenic mice**

441 A ~38.3cM genomic region (*i.e.*, *Cctq1*) spanning from *D7Mit318* (SSLP marker at 42.3 cM) to
442 *rs13479545* (SNP marker at 81.2 cM) was transferred from SJL/J mice (abbreviated throughout
443 as SJL; thick cornea) onto the genetic background of C57BLKS/J mice (abbreviated throughout
444 as KS; thin cornea) by reiterative backcrossing. Mice carrying the SJL alleles within the region
445 (*i.e.*, KS.SJL-*Cctq1*^{Het}) were selected at each generation by using a panel of six markers that
446 were tested and found to be polymorphic between KS and SJL mice. At the N10 generation,
447 mice were intercrossed. At this point, *Cctq1* was treated as a digenic locus, renamed to *Cctq1a*
448 and *Cctq1b* (see Results and Figure 2). *Cctq1a* encompassed the region spanning from
449 *D7Mit318* (42.3 cM) to *D7Mit220* (55.7 cM). *Cctq1b* spanned from *D7Mit105* (70.3 cM) to
450 *rs13479545* (81.2 cM). All genotype combinations of *Cctq1a* and *Cctq1b* (9 possible
451 combinations; *i.e.*, homozygosity for KS alleles, heterozygous, or homozygosity for SJL alleles
452 at each locus) were analyzed for their effect on CCT.

453

454 Sub-congenic mice harboring reduced *Cctq1a* intervals (KS alleles at *Cctq1b*) were also
455 generated. At N12, *Cctq1a* was reduced to a 15.9 cM region spanning from *D7mit347* to
456 *D7mit321*. These N12 sub-congenic mice are referred to throughout as KS.SJL-
457 *Cctq1a*(15.9cM). At N15, *Cctq1a* was reduced to a 9.9 cM region spanning from *rs3672782* to
458 *D7mit321*. These sub-congenic N15 mice are referred to throughout as KS.SJL-*Cctq1a*(9.9cM).
459 Sub-congenic mice were intercrossed, and all genotypes were assessed for the CCT
460 phenotype. The KS.SJL-*Cctq1* line has been sperm cryopreserved.

461

462 **CCT phenotyping**

463 All measurements were recorded from adult mice. Mice were injected with a standard mixture of
464 ketamine/xylazine (intraperitoneal injection of 100 mg ketamine + 10 mg xylazine / kg body
465 weight). During induction of anesthesia, mice were provided supplemental indirect warmth by a
466 heating pad. Immediately following anesthesia, eyes were hydrated with balanced salt solution
467 (BSS) and corneal images were obtained with a Bioptigen optical coherence tomographer (SD-
468 OCT; Bioptigen, Inc., USA). A 12mm telecentric bore was used to image the anterior segment of
469 each eye. The bore was positioned such that the pupil of the eye was centered in the volume
470 intensity projection. Scan parameters were as follows: radial volume scans 2.0 mm in diameter,
471 1000 A-scans/B-scan, 100 B-scans/volume, 1 frame/B-scan, and 1 volume. Central corneal
472 thickness (CCT) was measured for each eye using vertical angle-locked B-scan calipers. Mice
473 were included in the analysis if the difference between the right and left eyes was less than 7
474 μm and if both eyes were free from opacity. The average CCT with standard deviation for each
475 genotype was statistically compared using Student's two-tailed *t*-test for comparison of two
476 cohorts or one-way ANOVA with a Tukey post-test for comparison of three or more cohorts.

477

478 **Recombination mapping**

479 For genetic mapping of the gene underlying *Cctq1a*, additional polymorphic markers were
480 identified and tiled into the region. Intercrosses of N10 mice were continued and mice with
481 informative recombination events were analyzed for the CCT phenotype. Based on the allelic
482 effects of the QTL on the CCT phenotype (see Results), the genomic boundaries of the QTL
483 (and hence, the region of the underlying gene) were deduced by comparing the phenotype of
484 the recombinant mice with the location of the recombination event within the critical interval. The
485 following is a complete list of all the polymorphic markers used for genotyping (listed in order
486 from centromeric to telomeric): *D7Mit318*, *rs13479346*, *rs13479362*, *D7Mit347*, *D7Mit62*,
487 *rs6271685*, *rs108403472*, *Cctq1a-STR5*, *D7Mit31*, *rs3672782*, *rs32438580*, *rs3663323*,
488 *rs13479392*, *rs13479393*, *rs6247100*, *rs13479395*, *D7Mit301*, *D7Mit321*, *D7Mit220*, *D7Mit238*,
489 *D7Mit105*, *rs13479535*, *rs13479536*, and *rs13479545*. Primer sequences are available upon
490 request.
491
492 **Exome sequence analysis**
493 High quality genomic DNA was harvested from KS and SJL spleen tissue using a Qiagen
494 DNeasy Blood and Tissue kit following the manufacturer's instructions; an RNA digestion step
495 was included. DNA samples were sent to BGI Americas for sequencing and passed their quality
496 control standards. Libraries were constructed with an Agilent SureSelect 50Mb Mouse Exome
497 Capture Kit and were sequenced with 50X coverage using an Illumina HiSeq2000. Standard
498 bioinformatics analysis was conducted in which the data were filtered (by removing adaptor
499 contamination and low-quality reads from raw reads), aligned, and SNPs were called and
500 annotated using a reference genome (GRCm38 build).
501
502 **RNASeq analysis**
503 N12F3 KS.SJL-*Cctq1a(15.9cM)*^{KS}, KS.SJL-*Cctq1a(15.9cM)*^{SJL}, and KS inbred mice were
504 euthanized at three weeks of age by cervical dislocation. Immediately upon death, mice were

505 enucleated, and the eyes were placed in RNase free dishes containing RNA*later* RNA
506 stabilization reagent. Corneas from mice were dissected in RNA*later* and pooled to make one
507 sample (6 corneas per sample); three samples were collected per genotype. Cornea samples
508 were either stored at -80°C in RNA*later* or processed immediately. Corneas were transferred
509 from RNA*later* to 0.7 mL of lysis/binding buffer from the *mir*Vana miRNA isolation kit (Ambion)
510 and homogenized for 1 minute using a tissue tearer. The homogenate was then passed through
511 a QIAshredder column (Qiagen) and the lysate was collected. For the remainder of the
512 procedure, the samples were processed using the *mir*Vana kit for total RNA according to the
513 manufacturer's instructions. The quality and concentration of the RNA was analyzed using a
514 NanoDrop 2000 and the Agilent Model 2100 Bioanalyzer. All samples had RNA integrity
515 numbers of 9.5 or greater, indicating high quality RNA with little degradation of the samples.
516 Samples were barcoded and stranded libraries were prepared by the Genomics Division of the
517 Iowa Institute of Human Genetics. The nine libraries were pooled together, split into two equal
518 parts, and run on two lanes of an Illumina HiSeq to obtain 100 base pair, paired-end sequence
519 reads.
520
521 Reads were mapped to the mm10 mouse genome build using Tophat2 (ver 2.0.11[61]). The '-r'
522 parameter was set to 135, and the '--no-coverage-search' option was used. Transcript
523 abundance was quantified using Cufflinks (ver. 2.1[62]) for RefSeq transcript models from the
524 Illumina iGenomes mm10 package. Ribosomal RNA and mitochondrial gene loci, obtained from
525 USCS Genome Table Viewer, were masked from the Cufflinks analysis, and the '--max-bundle-
526 frags' parameter was set to 20000000. Differential expression between genotypes was
527 performed using Cuffdiff (ver. 2.1.1[63]). Genes identified from each comparison were
528 subsequently filtered for only those with a q-value ≤ 0.001 and a mean FPKM (Fragments Per
529 Kilobase of transcript per Million mapped reads) value ≥ 1 in at least one of the strains.
530 Functional enrichment analysis was performed with WebGestalt [32, 33] with analysis

531 parameters detailed in Supplementary Data 8.

532

533 **Constructing *Ctsc* null mice**

534 B6-*Ctsc*^{KO} mice were generated by the Genome Editing Facility at The University of Iowa on a
535 pure C57BL/6J (JAX Stock No. 000664) background by targeting *Ctsc* Exon 1 with
536 CRISPR/Cas9 using guide sequence: CGTGCGCTCCGACACTCCTGCC. Founders were
537 crossed with C57BL/6J mice and offspring analyzed for germline transmission of *Ctsc*
538 mutations. From four founders, we observed transmission of four separate *Ctsc* mutations, all
539 predicted to be null based on Sanger sequencing results. Four *Ctsc* mutations were propagated
540 in separate intercross mouse lines and were validated as null mutations by Western Blot using
541 an antibody against CTSC (Catalog #AF1034; R&D Systems, Inc.; Minneapolis, MN;
542 Supplementary Data 10). One of these mutations, *Ctsc*^{tm1Mga}, is a 46 bp exon 1 coding
543 sequence deletion that was used for additional downstream analysis.

544

545 **Constructing *Tyr* null mice**

546 To generate mice with *Tyr* null mutations on a pure C57BL/6J (JAX Stock No. 000664)
547 background, the Genome Editing Facility at the University of Iowa targeted *Tyr* Exon 1 with
548 CRISPR/Cas9 using two guide sequences simultaneously: 1) CCATGGATGGGTGATGGGAG
549 and 2) TTCAAAGGGGTGGATGACCG. Founders were crossed with C57BL/6J mice and
550 offspring analyzed by Sanger sequencing for germline transmission of *Tyr* mutations. This
551 experiment generated more alleles than we could reasonably work with (15 unique mutations
552 identified via sequencing; Supplementary Data 12). For each unique mutation, we set up a
553 complementation cross with B6.*Tyr*$^{c-2J}$ and screened progeny coat color for alleles conferring
554 novel function. F1 progeny were screened for 14 alleles; the mice harboring the remaining allele
555 did not produce F1 progeny. All 14 alleles produced a standard albino coat color in trans with
556 the *Tyr*$^{c-2J}$ mutation, indicating failure to complement. Going forward, we chose to complete

557 additional studies for one allele, *Tyr*^{tm4Mga}, which is a 4 bp deletion in the coding sequence of
558 exon 1, causes a frameshift and leads to a premature stop codon predicted to cause RNA-
559 mediated decay (i.e., a presumed null mutation). Accordingly, homozygotes of this strain are
560 albino.
561
562 **L-DOPA supplementation studies**
563 Breeder cages of C57BL/6J, B6.Cg-*Tyr*$^{c-2J}$/J, and B6.Cg-*Tyr*$^{c-h}$/J were provided with water
564 bottles containing water only (control) or water with 200mg/L of L-DOPA, with 30mg/L of
565 benserazide to minimize the conversion of L-DOPA to dopamine in the peripheral nervous
566 system. Fresh water bottles were prepared and supplied every Monday, Wednesday, and
567 Friday. Litters were weaned into cages where they continued to receive the same treatment of
568 supplemented water until 13–16 weeks old.
569
570 **Environmental chamber**
571 Breeder cages of C57BL/6J, B6.Cg-*Tyr*$^{c-2J}$/J, and B6.Cg-*Tyr*$^{c-h}$/J were housed in rodent
572 environmental control chambers (Powers Scientific) either at 10°C or 32°C and with either a
573 standard light cycle (12 h on/12 h off) or dark-rearing. Resulting pups were born and group-
574 housed at the altered temperature and light cycle until adulthood, when CCT was analyzed by
575 OCT at 10–15 weeks old.
576
577 **Axial length phenotyping**
578 Envisu R4300 spectral-domain optical coherence tomography (SD-OCT, Leica/Bioptigen Inc.,
579 Research Triangle Park, NC, USA) was employed to measure the ocular axial length in adult
580 (12-week-old) mice[64]. Mice were anesthetized with ketamine/xylazine (100 mg/kg and 5mg/kg,
581 respectively; intraperitoneal) and their eyes dilated before placing the animal in a cylindrical
582 holder. The eye was hydrated with Genteal (Alcon, Fort Worth, TX, USA) and positioned in front

583 of the OCT light source. Correct alignment of the eye was achieved by placing the Purkinje
584 image in the center of the pupil. The images were acquired in rectangular volume and radial
585 volume scans. The axial length was calculated by measuring the distance from the anterior
586 corneal surface to the RPE/choroid interface for both the left and right eyes of a given mouse.
587 Measurements from the left and right eye of each mouse were averaged to give a single
588 measurement per animal. Measurements from all eyes were included in the analysis. To
589 minimize the possible effect of body weight on ocular size, we ensured that body weight of
590 littermates was within a narrow range in each of the comparative groups. The average axial
591 length with standard deviation for each genotype was statistically compared using Student's
592 two-tailed *t*-test.
593
594 **Statistics**
595 A multiple regression analysis, in which each locus and the interaction component were
596 sequentially dropped from the 2-QTL model, was used to analyze the presence of two
597 interacting loci on chromosome 7. Student's two-tailed *t*-test was used to evaluate the difference
598 between two independent genotypes for CCT (*t*-values and degrees of freedom for each
599 comparison are listed in Supplementary Data 5) and axial length (*t*-value = 5.415; degrees of
600 freedom = 38). A one-way ANOVA with a Tukey post-test was used to evaluate the difference
601 between three or more independent genotypes for CCT (*f*-values and degrees of freedom for
602 each comparison are listed in Supplementary Data 5). A one-way ANOVA with Sidak test was
603 used to evaluate four comparisons to determine the effect of two environmental conditions on
604 CCT in B6.cg-$Tyr^{c\text{-}h}$ and B6.cg-$Tyr^{c\text{-}2J}$ mice (f-value and degrees of freedom are listed in
605 Supplementary Data 5).
606
607 **ACKNOWLEDGEMENTS**

608 This work was supported in part by Merit Review Award (101RX001481) from the U.S.
609 Departments of Veterans Affairs RR&D Service to MGA and by internal faculty development
610 funds to MGA. DRL was supported in part by a NIH/NEI training grant, EY021436. AHB was
611 supported in part by a NIH/NIDDK training grant, DK112751. Equipment maintenance was
612 supported in part by the University of Iowa Multidisciplinary Investigations in Visual Science
613 service cores (a resource supported by a P30 grant from the NIH/NEI to the University of Iowa,
614 EY025580). We acknowledge use of the University of Iowa Genome Editing Core Facility (a
615 core resource supported in part by grants from the NIH and from the Roy J. and Lucille A.
616 Carver College of Medicine) directed by William Paradee, PhD, and we thank Norma Sinclair,
617 Patricia Yarolem and Joanne Schwarting for their technical expertise in generating transgenic
618 mice. The authors thank Karl Broman for analyzing chromosome 7 of our original F2 dataset
619 with us. The contents do not represent the views of the U.S. Department of Veterans Affairs or
620 the U.S. Government.
621
622 The authors declare no competing interests.
623
624 **AUTHOR CONTRIBUTIONS**
625 K.J.M., D.R.L., and M.G.A. conceived and designed the experiments. K.J.M., D.R.L., C.J.V.,
626 A.H.B., L.M.D., N.P., H.E.M., M.N.A., and M.G.A. performed the experimental work. K.J.M.,
627 D.R.L., and M.G.A. performed experimental data analysis and interpreted the results with
628 contributions from all authors. S.S.W. analyzed the RNA-seq data supervised by T.E.S. W.J.P.
629 constructed the transgenic mice. S.K. performed the axial length experiment supervised by
630 K.S.N. K.W. verified and performed statistical analyses. K.J.M., D.R.L. and M.G.A. wrote the
631 manuscript with input from all authors. M.G.A. supervised the study and provided funding.
632

633 **REFERENCES**

634 1 Pediatric Eye Disease Investigator, G. *et al.* Central corneal thickness in children. *Arch*
635 *Ophthalmol* **129**, 1132-1138, doi:10.1001/archophthalmol.2011.225 (2011).
636 2 Hashmani, N. *et al.* Effect of age, sex, and refractive errors on central corneal thickness
637 measured by Oculus Pentacam((R)). *Clin Ophthalmol* **11**, 1233-1238,
638 doi:10.2147/OPTH.S141313 (2017).
639 3 Tayyab, A., Masrur, A., Afzal, F., Iqbal, F. & Naseem, K. Central Corneal Thickness and
640 its Relationship to Intra-Ocular and Epidmiological Determinants. *J Coll Physicians Surg*
641 *Pak* **26**, 494-497, doi:2349 (2016).
642 4 Brandt, J. D., Beiser, J. A., Kass, M. A., Gordon, M. O. & Ocular Hypertension
643 Treatment Study, G. Central Corneal Thickness in the Ocular Hypertension Treatment
644 Study (OHTS). *Ophthalmology* **127**, S72-S81, doi:10.1016/j.ophtha.2020.01.028 (2020).
645 5 La Rosa, F. A., Gross, R. L. & Orengo-Nania, S. Central corneal thickness of Caucasians
646 and African Americans in glaucomatous and nonglaucomatous populations. *Arch*
647 *Ophthalmol* **119**, 23-27 (2001).
648 6 Swierkowska, J. & Gajecka, M. Genetic factors influencing the reduction of central
649 corneal thickness in disorders affecting the eye. *Ophthalmic Genet* **38**, 501-510,
650 doi:10.1080/13816810.2017.1313993 (2017).
651 7 Toh, T. *et al.* Central corneal thickness is highly heritable: the twin eye studies.
652 *Investigative ophthalmology & visual science* **46**, 3718-3722, doi:10.1167/iovs.04-1497
653 (2005).
654 8 Zheng, Y. *et al.* Heritability of central corneal thickness in Chinese: the Guangzhou Twin
655 Eye Study. *Investigative ophthalmology & visual science* **49**, 4303-4307,
656 doi:10.1167/iovs.08-1934 (2008).
657 9 Choquet, H. *et al.* A multiethnic genome-wide analysis of 44,039 individuals identifies
658 41 new loci associated with central corneal thickness. *Commun Biol* **3**, 301,
659 doi:10.1038/s42003-020-1037-7 (2020).
660 10 Iglesias, A. I. *et al.* Cross-ancestry genome-wide association analysis of corneal thickness
661 strengthens link between complex and Mendelian eye diseases. *Nat Commun* **9**, 1864,
662 doi:10.1038/s41467-018-03646-6 (2018).
663 11 Dhooge, T. *et al.* More than meets the eye: Expanding and reviewing the clinical and
664 mutational spectrum of brittle cornea syndrome. *Hum Mutat*, doi:10.1002/humu.24199
665 (2021).
666 12 Lu, Y. *et al.* Genome-wide association analyses identify multiple loci associated with
667 central corneal thickness and keratoconus. *Nature genetics* **45**, 155-163,
668 doi:10.1038/ng.2506 (2013).
669 13 Lu, Y. *et al.* Common genetic variants near the Brittle Cornea Syndrome locus ZNF469
670 influence the blinding disease risk factor central corneal thickness. *PLoS Genet* **6**,
671 e1000947, doi:10.1371/journal.pgen.1000947 (2010).
672 14 Dimasi, D. P. *et al.* Novel quantitative trait loci for central corneal thickness identified by
673 candidate gene analysis of osteogenesis imperfecta genes. *Hum Genet* **127**, 33-44,
674 doi:10.1007/s00439-009-0729-3 (2010).
675 15 Zhang, J., Wu, D., Dai, Y. & Xu, J. Functional relevance for central cornea thickness-
676 associated genetic variants by using integrative analyses. *BioData Min* **11**, 19,
677 doi:10.1186/s13040-018-0179-3 (2018).

16 Lively, G. D., Koehn, D., Hedberg-Buenz, A., Wang, K. & Anderson, M. G. Quantitative trait loci associated with murine central corneal thickness. *Physiological genomics* **42**, 281-286, doi:10.1152/physiolgenomics.00140.2009 (2010).

17 Koehn, D. R., Meyer, K. J. & Anderson, M. G. Genetic Evidence for Differential Regulation of Corneal Epithelial and Stromal Thickness. *Invest Ophthalmol Vis Sci* **56**, 5599-5607, doi:10.1167/iovs.15-17179 (2015).

18 Lively, G. D. *et al.* Genetic Dependence of Central Corneal Thickness among Inbred Strains of Mice. *Investigative ophthalmology & visual science* **51**, 160-171, doi:10.1167/iovs.09-3429 (2010).

19 Broman, K. W. & Sen, S. *A Guide to QTL Mapping with R/qtl*. (Springer Science+Business Media, 2009).

20 Broman, K. W., Wu, H., Sen, S. & Churchill, G. A. R/qtl: QTL mapping in experimental crosses. *Bioinformatics* **19**, 889-890 (2003).

21 Wynn, E. H., Sanchez-Andrade, G., Carss, K. J. & Logan, D. W. Genomic variation in the vomeronasal receptor gene repertoires of inbred mice. *BMC Genomics* **13**, 415, doi:10.1186/1471-2164-13-415 (2012).

22 Liao, Y., Wang, J., Jaehnig, E. J., Shi, Z. & Zhang, B. WebGestalt 2019: gene set analysis toolkit with revamped UIs and APIs. *Nucleic acids research* **47**, W199-W205, doi:10.1093/nar/gkz401 (2019).

23 Wang, Y., Huso, D., Cahill, H., Ryugo, D. & Nathans, J. Progressive cerebellar, auditory, and esophageal dysfunction caused by targeted disruption of the frizzled-4 gene. *J Neurosci* **21**, 4761-4771 (2001).

24 Pham, C. T. & Ley, T. J. Dipeptidyl peptidase I is required for the processing and activation of granzymes A and B in vivo. *Proc Natl Acad Sci U S A* **96**, 8627-8632, doi:10.1073/pnas.96.15.8627 (1999).

25 Le Fur, N., Kelsall, S. R. & Mintz, B. Base substitution at different alternative splice donor sites of the tyrosinase gene in murine albinism. *Genomics* **37**, 245-248, doi:10.1006/geno.1996.0551 (1996).

26 Green, E. L. Albino-2J (c<2J>). *Mouse News Lett* **49** (1973).

27 Beermann, F., Orlow, S. J. & Lamoreux, M. L. The Tyr (albino) locus of the laboratory mouse. *Mamm Genome* **15**, 749-758, doi:10.1007/s00335-004-4002-8 (2004).

28 Zhou, X., Pardue, M. T., Iuvone, P. M. & Qu, J. Dopamine signaling and myopia development: What are the key challenges. *Prog Retin Eye Res* **61**, 60-71, doi:10.1016/j.preteyeres.2017.06.003 (2017).

29 Feldkaemper, M. & Schaeffel, F. An updated view on the role of dopamine in myopia. *Exp Eye Res* **114**, 106-119, doi:10.1016/j.exer.2013.02.007 (2013).

30 Bergen, M. A. *et al.* Altered Refractive Development in Mice With Reduced Levels of Retinal Dopamine. *Investigative ophthalmology & visual science* **57**, 4412-4419, doi:10.1167/iovs.15-17784 (2016).

31 Kidson, S. & Fabian, B. Pigment synthesis in the Himalayan mouse. *J Exp Zool* **210**, 145-152, doi:10.1002/jez.1402100116 (1979).

32 Kwon, B. S., Halaban, R. & Chintamaneni, C. Molecular basis of mouse Himalayan mutation. *Biochem Biophys Res Commun* **161**, 252-260, doi:10.1016/0006-291x(89)91588-x (1989).

33 Tkatchenko, T. V. *et al.* Photopic visual input is necessary for emmetropization in mice. *Exp Eye Res* **115**, 87-95, doi:10.1016/j.exer.2013.06.025 (2013).

34 Allen, G. M. The heredity of coat color in mice. *Proceedings of the American Academy of Arts and Sciences* **40**, 61-163 (1904).

35 Castle, W. E. & Allen, G. M. The heredity of albinism. *Proceedings of the American Academy of Arts and Sciences* **38**, 603-622 (1903).

36 Seruggia, D., Josa, S., Fernandez, A. & Montoliu, L. The structure and function of the mouse tyrosinase locus. *Pigment Cell Melanoma Res*, doi:10.1111/pcmr.12942 (2020).

37 Hanlon, S. D., Patel, N. B. & Burns, A. R. Assessment of postnatal corneal development in the C57BL/6 mouse using spectral domain optical coherence tomography and microwave-assisted histology. *Exp Eye Res* **93**, 363-370, doi:10.1016/j.exer.2011.04.013 (2011).

38 Chakraborty, R., Ostrin, L. A., Benavente-Perez, A. & Verkicharla, P. K. Optical mechanisms regulating emmetropisation and refractive errors: evidence from animal models. *Clin Exp Optom* **103**, 55-67, doi:10.1111/cxo.12991 (2020).

39 Mohawk, J. A., Green, C. B. & Takahashi, J. S. Central and peripheral circadian clocks in mammals. *Annu Rev Neurosci* **35**, 445-462, doi:10.1146/annurev-neuro-060909-153128 (2012).

40 Peirson, S. N., Brown, L. A., Pothecary, C. A., Benson, L. A. & Fisk, A. S. Light and the laboratory mouse. *J Neurosci Methods* **300**, 26-36, doi:10.1016/j.jneumeth.2017.04.007 (2018).

41 Steininger, T. L., Rye, D. B., Gilliland, M. A., Wainer, B. H. & Benca, R. M. Differences in the retinohypothalamic tract in albino Lewis versus brown Norway rat strains. *Neuroscience* **54**, 11-14, doi:10.1016/0306-4522(93)90379-t (1993).

42 Miller, A. M., Chappell, R., Obermeyer, W. H. & Benca, R. M. Analysis of the retinohypothalamic tract in congenic albino and pigmented rats. *Brain Res* **741**, 348-351, doi:10.1016/s0006-8993(96)01050-5 (1996).

43 Fleming, M. D., Benca, R. M. & Behan, M. Retinal projections to the subcortical visual system in congenic albino and pigmented rats. *Neuroscience* **143**, 895-904, doi:10.1016/j.neuroscience.2006.08.016 (2006).

44 Chakraborty, R. *et al.* Circadian rhythms, refractive development, and myopia. *Ophthalmic Physiol Opt* **38**, 217-245, doi:10.1111/opo.12453 (2018).

45 Lopez, V. M., Decatur, C. L., Stamer, W. D., Lynch, R. M. & McKay, B. S. L-DOPA is an endogenous ligand for OA1. *PLoS Biol* **6**, e236, doi:10.1371/journal.pbio.0060236 (2008).

46 Korshunov, K. S., Blakemore, L. J. & Trombley, P. Q. Dopamine: A Modulator of Circadian Rhythms in the Central Nervous System. *Front Cell Neurosci* **11**, 91, doi:10.3389/fncel.2017.00091 (2017).

47 Libby, R. T. *et al.* Modification of ocular defects in mouse developmental glaucoma models by tyrosinase. *Science* **299**, 1578-1581, doi:10.1126/science.1080095 (2003).

48 Lee, H., Scott, J., Griffiths, H., Self, J. E. & Lotery, A. Oral levodopa rescues retinal morphology and visual function in a murine model of human albinism. *Pigment Cell Melanoma Res* **32**, 657-671, doi:10.1111/pcmr.12782 (2019).

49 Kirkwood, B. J. Albinism and its implications with vision. *Insight* **34**, 13-16 (2009).

50 Rao, V. A., Swathi, P., Chaitra & Thappa, D. M. Bilateral keratoconus with oculocutaneous albinism. *Indian J Dermatol Venereol Leprol* **74**, 407-409, doi:10.4103/0378-6323.42929 (2008).

769 51 Dimasi, D. P. *et al.* Ethnic and mouse strain differences in central corneal thickness and
770 association with pigmentation phenotype. *PLoS One* **6**, e22103,
771 doi:10.1371/journal.pone.0022103 (2011).
772 52 Buttner, C. *et al.* Tyrosinase Is a Novel Endogenous Regulator of Developmental and
773 Inflammatory Lymphangiogenesis. *Am J Pathol* **189**, 440-448,
774 doi:10.1016/j.ajpath.2018.10.014 (2019).
775 53 Mason, C. & Slavi, N. Retinal Ganglion Cell Axon Wiring Establishing the Binocular
776 Circuit. *Annu Rev Vis Sci* **6**, 215-236, doi:10.1146/annurev-vision-091517-034306
777 (2020).
778 54 Savinova, O. V. *et al.* Intraocular pressure in genetically distinct mice: an update and
779 strain survey. *BMC Genet* **2**, 12, doi:10.1186/1471-2156-2-12 (2001).
780 55 Johnson, B. A., Cole, B. S., Geisert, E. E., Ikeda, S. & Ikeda, A. Tyrosinase is the
781 modifier of retinoschisis in mice. *Genetics* **186**, 1337-1344,
782 doi:10.1534/genetics.110.120840 (2010).
783 56 Anderson, M. G. *et al.* Genetic context determines susceptibility to intraocular pressure
784 elevation in a mouse pigmentary glaucoma. *BMC Biol* **4**, 20, doi:10.1186/1741-7007-4-
785 20 (2006).
786 57 Oh, J. *et al.* Genetic background-dependent role of Egr1 for eyelid development. *Proc*
787 *Natl Acad Sci U S A* **114**, E7131-E7139, doi:10.1073/pnas.1705848114 (2017).
788 58 Mott, R. & Flint, J. Dissecting quantitative traits in mice. *Annual review of genomics and*
789 *human genetics* **14**, 421-439, doi:10.1146/annurev-genom-091212-153419 (2013).
790 59 Solberg Woods, L. C. QTL mapping in outbred populations: successes and challenges.
791 *Physiological genomics* **46**, 81-90, doi:10.1152/physiolgenomics.00127.2013 (2014).
792 60 Meyer, K. J. & Anderson, M. G. Genetic modifiers as relevant biological variables of eye
793 disorders. *Hum Mol Genet* **26**, R58-R67, doi:10.1093/hmg/ddx180 (2017).
794 61 Kim, D. *et al.* TopHat2: accurate alignment of transcriptomes in the presence of
795 insertions, deletions and gene fusions. *Genome Biol* **14**, R36, doi:10.1186/gb-2013-14-4-
796 r36 (2013).
797 62 Trapnell, C. *et al.* Transcript assembly and quantification by RNA-Seq reveals
798 unannotated transcripts and isoform switching during cell differentiation. *Nat Biotechnol*
799 **28**, 511-515, doi:10.1038/nbt.1621 (2010).
800 63 Trapnell, C. *et al.* Differential analysis of gene regulation at transcript resolution with
801 RNA-seq. *Nat Biotechnol* **31**, 46-53, doi:10.1038/nbt.2450 (2013).
802 64 Paylakhi, S. *et al.* Muller glia-derived PRSS56 is required to sustain ocular axial growth
803 and prevent refractive error. *PLoS Genet* **14**, e1007244,
804 doi:10.1371/journal.pgen.1007244 (2018).
805

806

807 **Figure 1. *Cctq1* contains two adjacent interacting QTL, *Cctq1a* and *Cctq1b*. a** Heatmap of
808 the chromosome 7 pairwise scan. The *upper left triangle* displays the interactive LOD score
809 (LOD_i; left side of the heat map scale) and the *lower right triangle* displays the full LOD score
810 (LOD_f; right side of the heat map scale). Chromosome 7 positions (Mb) are based on NCBI
811 Build 33. **b** Genetic map of chromosome 7 showing the *Cctq1a* and *Cctq1b* loci. The area *boxed*
812 *in red* is the original *Cctq1* interval blown up to show the intervals of *Cctq1a* and *Cctq1b*, and a
813 subset of the polymorphic markers used for genotyping. The *arrows* indicate the peaks of the
814 two QTL.
815

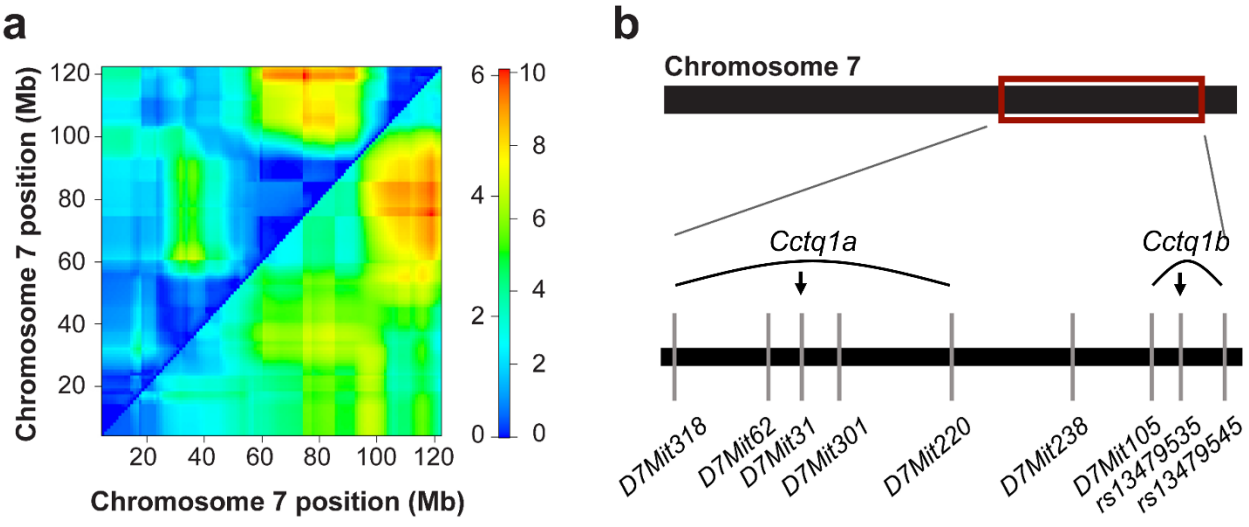

816

817 **Table 1. CCT phenotype results of adult N10F2 mice.**

818

Cctq1a[a]	*Cctq1b*[a]	Avg. CCT ± StDev.[b]	# Mice
KS	KS	94.8 ± 2.4	13
KS	Het	93.3 ± 2.5	13
KS	SJL	90.8 ± 2.6	13
Het	KS	95.5 ± 2.9	13
Het	Het	96.2 ± 3.4	13
Het	SJL	97.0 ± 2.3	13
SJL	KS	88.1 ± 3.7*	13
SJL	Het	86.8 ± 4.2*	13
SJL	SJL	88.8 ± 3.6*	13

819

820 [a] KS, homozygous for KS alleles across the indicated QTL; Het, heterozygous for alleles across

821 the indicated QTL; SJL, homozygous for SJL alleles across the indicated QTL

822 [b] Asterisk (*), significantly different ($p < 0.01$) than inbred KS mice by one-way ANOVA with

823 Tukey post-test

824 **Figure 2. Genetic mapping of *Cctq1a* on mouse chromosome 7 using intercrosses of**
825 **KS.SJL-*Cctq1a* congenic and sub-congenic mice.** *Black boxes* represent the KS or HET
826 genotype associated with a thick cornea and *white boxes* represent the SJL genotype
827 associated with a thin cornea. The number of mice (*n*) with each haplotype is listed to the left of
828 each row, with progeny-tested mice denoted with an asterisk (*). The adult CCT phenotype
829 (*pheno*; measured by optical coherence tomography) relative to littermate controls and the
830 deduced genotype (*geno*) for each haplotype is listed to the right of each row as “Thick KS” or
831 “Thin SJL”. The *vertical lines* across the chromosome represent markers that are polymorphic
832 between KS and SJL mice. *Black arrowheads* indicate partial genes.
833

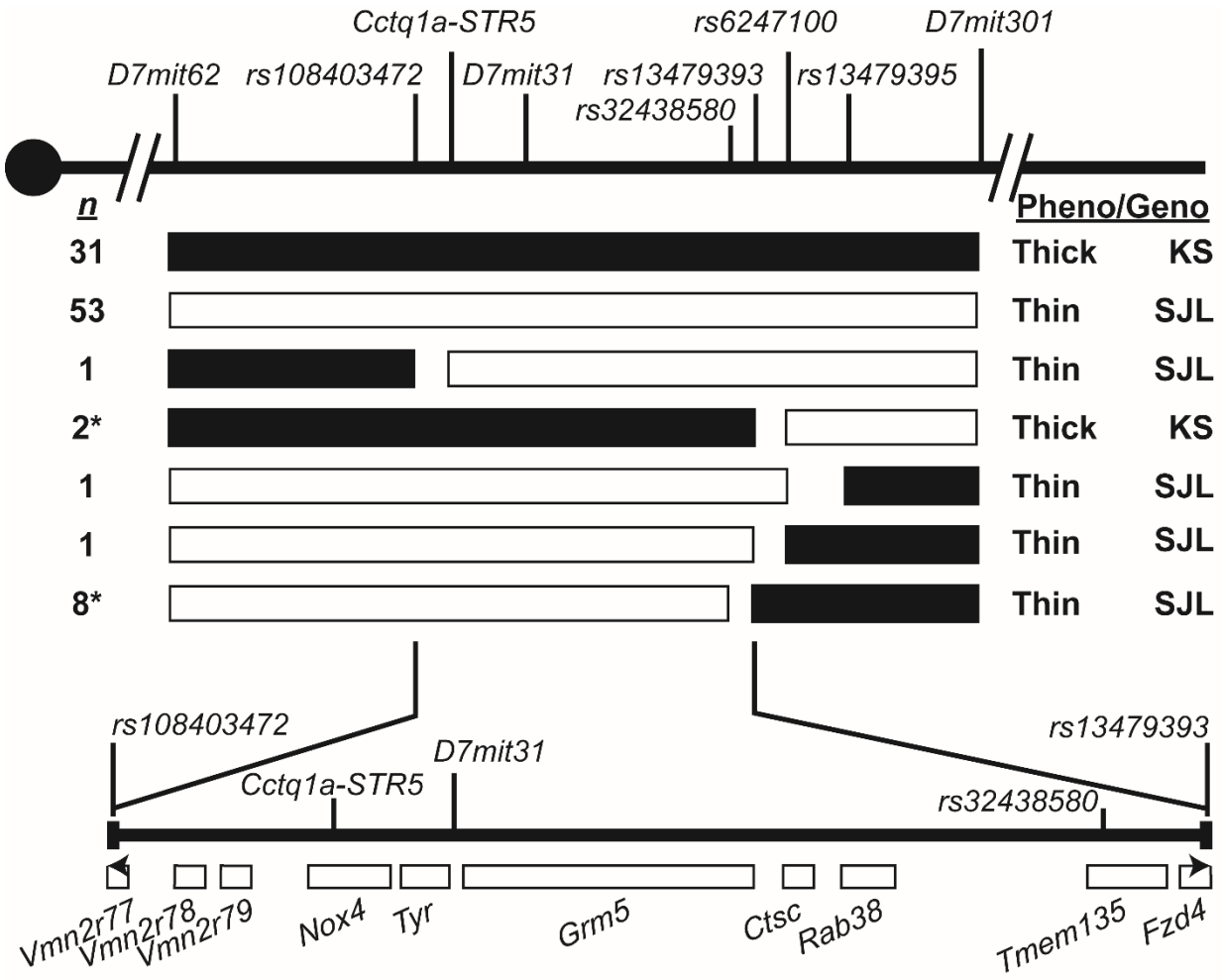
Cctq1a-STR5
rs6247100
D7mit301
D7mit62
rs108403472
D7mit31
rs13479393
rs32438580
rs13479395
n
Pheno/Geno
31
Thick
KS
53
Thin
SJL
1
Thin
SJL
2*
Thick
KS
1
Thin
SJL
1
Thin
SJL
8*
Thin
SJL
rs108403472
D7mit31
Cctq1a-STR5
rs13479393
rs32438580
Vmn2r77
Vmn2r78
Vmn2r79
Nox4
Tyr
Grm5
Ctsc
Rab38
Tmem135
Fzd4

834

835 **Figure 3. Testing the influence of *Cctq1a* positional candidate genes on central corneal**
836 **thickness (CCT).** Each point on the graph represents the average CCT measured by optical
837 coherence tomography from one adult mouse with age-matching across genotypes and *error*
838 *bars* = mean ± standard deviation. **a** Plot comparing CCT for *Cctq1a*^{KS} vs. *Cctq1a*^{SJL} genotypes
839 in KS.SJL-*Cctq1a* N15F7 sub-congenic littermate mice 12 to13 weeks old (Student's two-tailed
840 *t*-test). **b** Plot comparing CCT between *Fzd4* genotypes for littermate mice 12 to 13 weeks old
841 (one-way ANOVA with Tukey test). **c** Plot comparing the CCT for mice with a *Fzd4*^{tm1Nat} allele in
842 trans with a *Cctq1a*^{SJL} allele to littermate controls having a *Fzd4*^{WT} allele in trans with a
843 *Cctq1a*^{SJL} allele (Student's two-tailed *t*-test; 17 to 33 weeks old). **d** Plot comparing CCT between
844 *Ctsc*^{tm1Ley} genotypes for 11-week-old littermate mice (one-way ANOVA with Tukey test). **e** Plot
845 comparing CCT for mice with a *Ctsc*^{tm1Ley} allele in trans with a *Cctq1a*^{SJL} allele compared to
846 littermate controls having a *Ctsc*^{tm1Ley} allele in trans with a *Cctq1a*^{KS} allele (Student's two-tailed *t*-
847 test; 15 to18 weeks old). **f** Plot comparing CCT for mice harboring one of four *Ctsc*^{KO} alleles on
848 a pure B6 background to littermate controls (one-way ANOVA with Tukey test; 10 to 12 weeks
849 old). **g** Plot comparing CCT for mice with a *Ctsc*^{tm1Mga} allele, made on a pure B6 background, in
850 trans with a *Cctq1a*^{SJL} allele to littermate controls having a *Ctsc*^{WT} allele in trans with a *Cctq1a*^{SJL}
851 allele (Student's two-tailed *t*-test; 10 to 11 weeks old). **h** Plot comparing CCT for B6.*Tyr*$^{c-2J}$ mice
852 to B6 mice (Student's two-tailed *t*-test; 11 to 13 weeks old). **i** Plot comparing CCT for mice with
853 a *Tyr*$^{c-2J}$ allele in trans with a *Cctq1a*^{SJL} allele to littermate controls having a *Tyr*$^{c-2J}$ allele in trans
854 with a *Cctq1a*^{KS} allele (Student's two-tailed *t*-test; 10 to 12 weeks old).

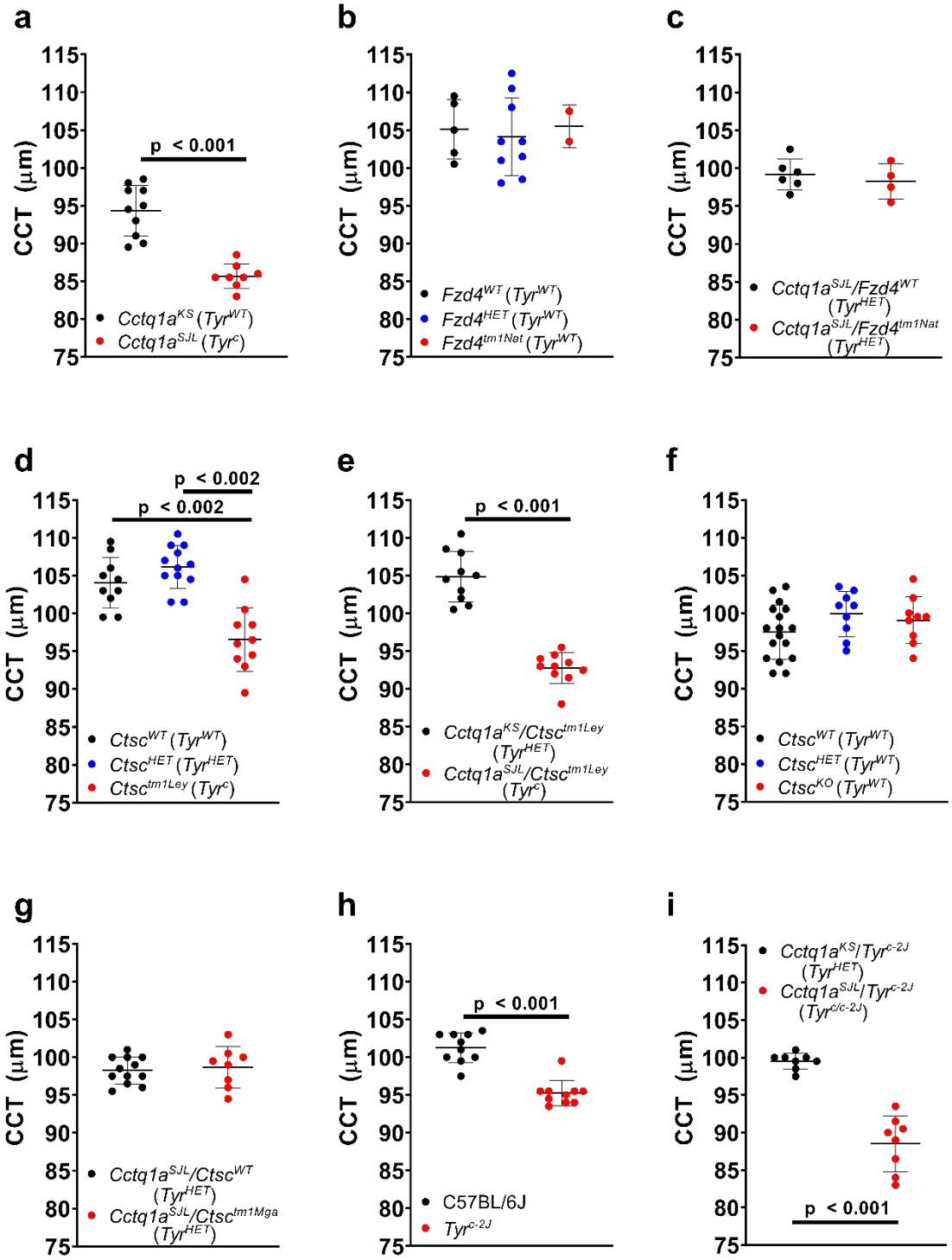
a
b
c
d
e
f
g
h
i
CCT (μm)
115
110
105
100
95
90
85
80
75
p < 0.001
p < 0.002
p < 0.002
p < 0.001
p < 0.001
p < 0.001
Cctq1a^KS (Tyr^WT)
Cctq1a^SJL (Tyr^c)
Fzd4^WT (Tyr^WT)
Fzd4^HET (Tyr^WT)
Fzd4^tm1Nat (Tyr^WT)
Cctq1a^SJL/Fzd4^WT (Tyr^HET)
Cctq1a^SJL/Fzd4^tm1Nat (Tyr^HET)
Ctsc^WT (Tyr^WT)
Ctsc^HET (Tyr^HET)
Ctsc^tm1Ley (Tyr^c)
Cctq1a^KS/Ctsc^tm1Ley (Tyr^HET)
Cctq1a^SJL/Ctsc^tm1Ley (Tyr^c)
Ctsc^WT (Tyr^WT)
Ctsc^HET (Tyr^WT)
Ctsc^KO (Tyr^WT)
Cctq1a^SJL/Ctsc^WT (Tyr^HET)
Cctq1a^SJL/Ctsc^tm1Mga (Tyr^HET)
C57BL/6J
Tyr^c-2J
Cctq1a^KS/Tyr^c-2J (Tyr^HET)
Cctq1a^SJL/Tyr^c-2J (Tyr^c/c-2J)

855

856 **Figure 4. The influence of a null *Tyr* mutation on central corneal thickness (CCT).** Each
857 point on the graph represents the average CCT measured by optical coherence tomography
858 from one adult mouse, 13 to 17 weeks old, with age-matching across genotypes and *error bars*
859 = mean ± standard deviation. The plot compares CCT between mice homozygous for the
860 Tyr^{tm4Mga} allele on a pure B6 background to littermate controls with heterozygous (HET) or wild-
861 type (WT) alleles (one-way ANOVA with Tukey test).
862

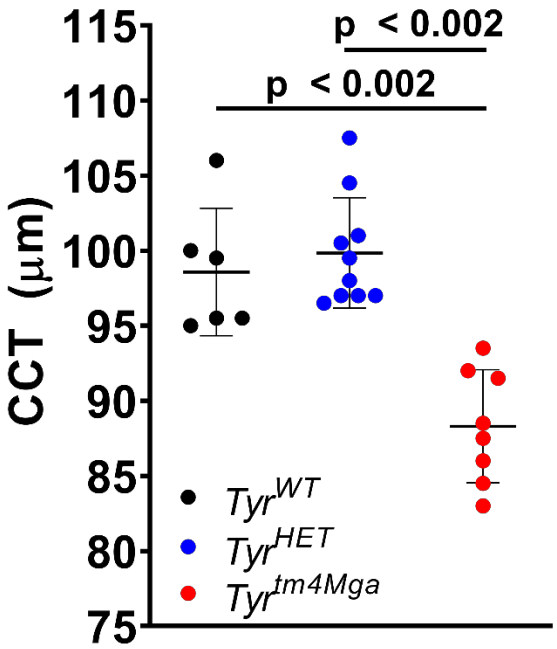

863
864

1 **Figure 5. Testing the influence of DOPA on central corneal thickness (CCT).** Each point on the graph represents the average

2 CCT measured by optical coherence tomography from one adult mouse, 13 to 16 weeks old, with age-matching across genotypes

3 and *error bars* = mean ± standard deviation. Plots compare CCT between mice supplied with DOPA in the drinking water from

4 conception through 10-weeks-old to controls supplied with standard drinking water for the **a** B6, **b** B6.*Tyr*$^{c\text{-}h}$, and **c** B6.*Tyr*$^{c\text{-}2J}$ strains of

5 mice (Student's two-tailed *t*-test for each comparison).

6

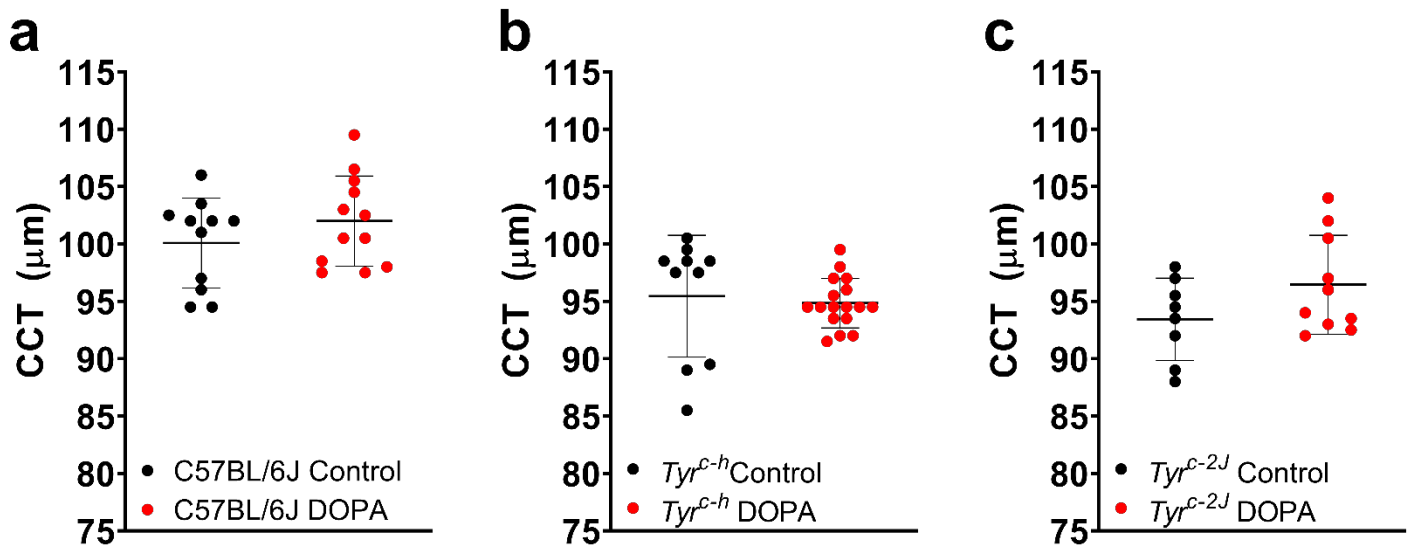

7

Figure 6. The influence of temperature and light on central corneal thickness (CCT) for the B6, B6.*Tyr*$^{c\text{-}h}$, and B6.*Tyr*$^{c\text{-}2J}$ strains of mice. Each point on the graph represents the average CCT measured by optical coherence tomography from one adult mouse, 10 to 15 weeks old, with age-matching across genotypes and *error bars* = mean ± standard deviation. Cohorts were subjected to standard lighting or dark-rearing. Each grouping of *Tyr* genotypes (WT B6 = *black*; *c-h* temperature-sensitive himalayan = *blue*; *c-2J* albino = *red*) has mice raised at 10°C or 32°C (one-way ANOVA with Sidak test).

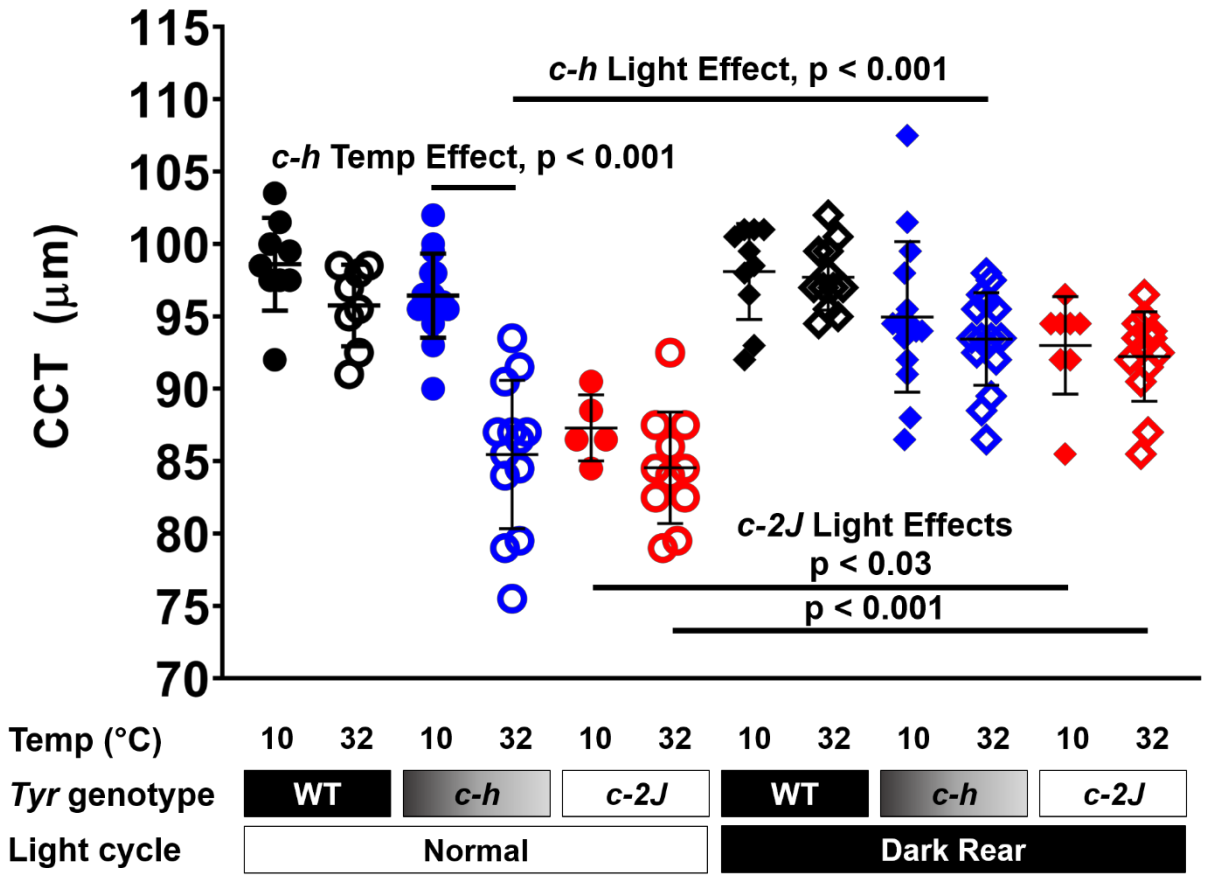
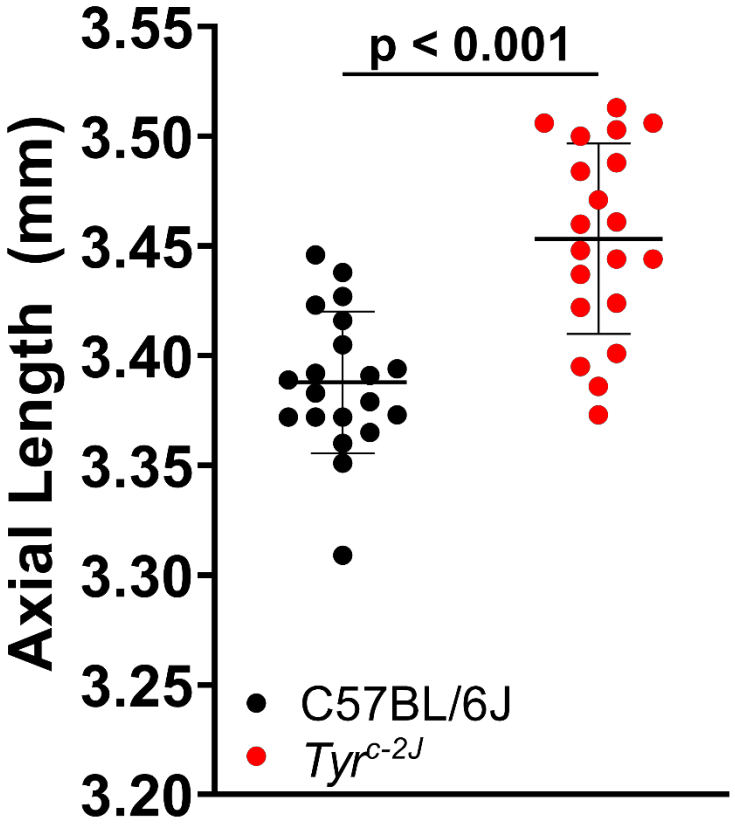
Figure 7. The influence of *Tyr* on ocular axial length. Each point on the graph represents the average axial length measured by optical coherence tomography from one 12-week-old adult mouse and *error bars* = mean ± standard deviation. The plot compares axial length between the B6 and B6.*Tyr*$^{c\text{-}2J}$ strains of mice, measured from the outer surface of the cornea to the retinal pigment epithelium/choroid interface (Student's two-tailed *t*-test).